Detailing organelle division and segregation in *Plasmodium falciparum*

Julie M.J. Verhoef[1], Cas Boshoven[1], Felix Evers[1], Laura J. Akkerman[1], Barend C.A. Gijsbrechts[1], Marga van de Vegte-Bolmer[1], Geert-Jan van Gemert[1], Akhil B. Vaidya[2], Taco W.A. Kooij[1*]

[1]Department of Medical Microbiology, Radboudumc Center for Infectious Diseases, Radboud University Medical Center, Nijmegen, The Netherlands
[2]Center for Molecular Parasitology, Institute for Molecular Medicine and Infectious Disease, Department of Microbiology and Immunology, Drexel University College of Medicine, Philadelphia, USA

*Corresponding author: Taco.Kooij@radboudumc.nl

Abstract

The malaria causing parasite, *P. falciparum*, replicates through a tightly orchestrated process termed schizogony, where approximately 32 daughter parasites are formed in a single infected red blood cell and thousands of daughter cells in mosquito- or liver-stages. One-per-cell organelles, such as the mitochondrion and apicoplast, need to be properly divided and segregated to ensure a complete set of organelles per daughter parasites. Although this is highly essential, details about the processes and mechanisms involved remain unknown. We developed a new reporter parasite line that allows visualization of the mitochondrion in blood- and mosquito stages. Using high-resolution 3D-imaging, we found that the mitochondrion orients in a cartwheel structure, prior to stepwise, non-geometric division during the last stage of schizogony. Analysis of focused ion beam scanning electron microscopy (FIB-SEM) data confirmed these mitochondrial division stages. Furthermore, these data allowed us to elucidate apicoplast division steps, highlighted its close association with the mitochondrion, and showed putative roles of the centriolar plaques (CPs) in apicoplast segregation. These observations form the foundation for a new detailed model of mitochondrial and apicoplast division and segregation during *P. falciparum* schizogony and pave the way for future studies into the mechanisms of organelle division and segregation.

Introduction

Malaria is a devastating parasitic disease causing 247 million cases resulting in 619,000 deaths in 2021, especially in children under 5 years old[1]. *Plasmodium falciparum* is the most virulent parasite species causing malaria. Continued emergence of resistant parasites to antimalarial drugs is a major problem for global malaria control and necessitates continued development of novel antimalarials.

The malaria parasite harbors a unique mitochondrion that differs greatly from its host mitochondrion at a molecular and functional level[2]. While the most prominent role of the mitochondrion in humans is respiration and consequent energy conversion, in the disease-causing asexual blood-stages of *P. falciparum* the respiratory chain appears to be exclusively essential to support pyrimidine biosynthesis[3]. It is only during preparation for transition to the mosquito vector where sexual reproduction takes place, that canonical mitochondrial functions such as the tricarboxylic acid cycle (TCA) cycle and the oxidative phosphorylation (OXPHOS) pathway become more abundant and critical[4,5]. Because of these differences, it is not surprising that this organelle is the drug target of several anti-malarial compounds, such as atovaquone, DSM265, proguanil and ELQ300[6,7].

Host and stage transitions are commonplace in the complicated life cycle of *Plasmodium* parasites. During erythrocytic asexual replication, one parasite is segmented into approximately 32 merozoites through a tightly orchestrated process called schizogony. Schizogony happens on a much larger scale in mosquito and liver stages, where one parasite is divided into thousands or even tens of thousands of daughter parasites. *P. falciparum* harbors only a single mitochondrion during these stages, which needs to be properly divided and distributed among the daughter cells[8]. During parasite development in asexual blood stages, the tubular mitochondrion elongates and forms a large, branched network that stretches throughout the parasite[9]. Only during the final stages of schizogony, once nuclear division is completed, does the mitochondrion undergo rapid fission[10]. The apicoplast, another essential single copy organelle of secondary endosymbiotic origin, forms a comparable branched network, but divides prior to mitochondrial fission during blood- and liver-stage replication[9,11]. To produce viable offspring, the parasite has to ensure that each daughter parasite has a complete set of these organelles. However, so far a detailed view of these processes and the mechanisms involved is lacking.

We aimed to capture the process of mitochondrial division in detail using different imaging methods. However, this comes with several challenges. Firstly, imaging the small-sized parasites (1-7 µm diameter), and the even smaller organelles within the parasites, requires the use of super-resolution imaging techniques. Secondly, visualization of the mitochondrion requires a specific fluorescent marker or dye. Mitochondrial dyes, such as Rhodamine123 and MitoTracker™, have been widely used in the field[12]. These dyes rely on membrane potential to enter the mitochondrion and are therefore also used as a viability marker[13]. However, some of these dyes were tested in a drug screen and shown to be highly active against *P. falciparum* with IC50 values below 200 nM[14,15]. Additionally, in our hands MitoTracker signal can be diffuse, and therefore limit the resolution that is needed for the visualization of mitochondrial fission. Hence, we aimed to develop a reporter parasite line which harbors a fluorescent mitochondrial marker that allows imaging of this organelle in live and fixed conditions in all life-cycle stages of *P. falciparum*. To do this, we deployed a similar strategy

that has been used successfully in the rodent model *Plasmodium berghei*[16,17]. The targeting signal of the known mitochondrial protein HSP70-3 was fused with a fluorescent protein and integrated in a silent intergenic locus (SIL)[18]. Expression of this mitochondrial-localized fluorescent protein allowed visualization of the organelle during imaging of asexual, sexual and mosquito stages. Using high resolution confocal microscopy, we were able to make a detailed 3D map of different mitochondrial fission stages during schizogony in asexual blood stages. Focused ion beam scanning electron microscopy (FIB-SEM) image stacks from Evers *et al.* were used to confirm these mitochondrial fission stages with high detail[19]. This also allowed us to study apicoplast division and highlighted the potential role of the centriolar plaques (CPs) in apicoplast segregation. These different microscopic approaches empowered us to put forward a detailed model for mitochondrial and apicoplast division and distribution during the final stages of schizogony.

Results

To acquire a detailed understanding of mitochondrial fission and distribution, we set out to capture this process throughout the *Plasmodium* life cycle by combining different microscopy approaches. We stained mature blood-stage wild-type *P. falciparum* NF54 strain parasites with two different MitoTracker dyes and used these to visualize the mitochondrion in fixed confocal imaging. Surprisingly, both MitoTracker dyes showed a discontinuous, punctuated staining pattern (Figure 1A). FIB-SEM studies have confirmed the prevailing notion that the mitochondrion is a single, branched network during these schizont stages[19]. While this observation may arise from crosslinking of the MitoTracker dyes to specific proteins and aggregations thereof resulting from the fixation process, we concluded that the punctuated staining pattern is likely an artifact and consequently limits our ability to dissect and visualize the process mitochondrial fission. To address this, we developed a new fluorescent mitochondrial marker that can be used for imaging live and fixed samples (Figure S1).

Design and generation of a new mitochondrial marker parasite line

We designed a mitochondrial marker that consists of the promotor and mitochondrial targeting sequence of the gene encoding the mitochondrial heat shock protein 70 (HSP70-3, PF3D7_1134000), fused to an mScarlet red fluorescent protein (Figure S1A). HSP70-3 was selected based on its high and consistent expression profile throughout the whole life cycle and has been successfully used for the same purpose in *P. berghei*[16,17]. We aimed to stably integrate this fluorescent marker in the *P. falciparum* genome, without affecting any normal biological processes and parasite growth throughout the parasite life cycle. Selection of the new integration site, SIL7, is described extensively in Supplemental Information S1. The integration plasmid was transfected into NF54 parasites together with two different Cas9 guide plasmids directed at the SIL7 site. Successful integration of the mitochondrial marker and absence of WT parasite contaminations were confirmed by integration PCR (Figure S1B). A growth assay showed no difference in growth of the mitochondrial reporter line, MitoRed, compared to WT parasites in asexual blood stages (Figure S1C).

Characterization of the MitoRed parasite line

To visualize the mitochondrial marker, asexual blood-stage MitoRed parasites were fixed and used for fluorescent imaging. The fluorescent signal was well preserved after fixation and no antibody staining was required for mitochondrial visualization in all asexual blood stages (Figure 1B). To assess whether the punctuated mitochondrial morphology observed after MitoTracker staining was an imaging artifact or a morphological aberration caused by the dye, we stained MitoRed parasites with three different MitoTracker dyes. Discontinuous, punctuated mitochondria were observed in all MitoRed parasites stained with MitoTracker, while this was not observed in unstained MitoRed parasites (Figure 1C). The effect was less pronounced during live imaging of MitoTracker stained parasites (Figure S2). While there is an obvious imaging artifact following fixation of MitoTracker-stained blood-stage *P. falciparum* parasites, the altered MitoRed signal in the presence of the dye might even suggest possible changes in mitochondrial morphology.

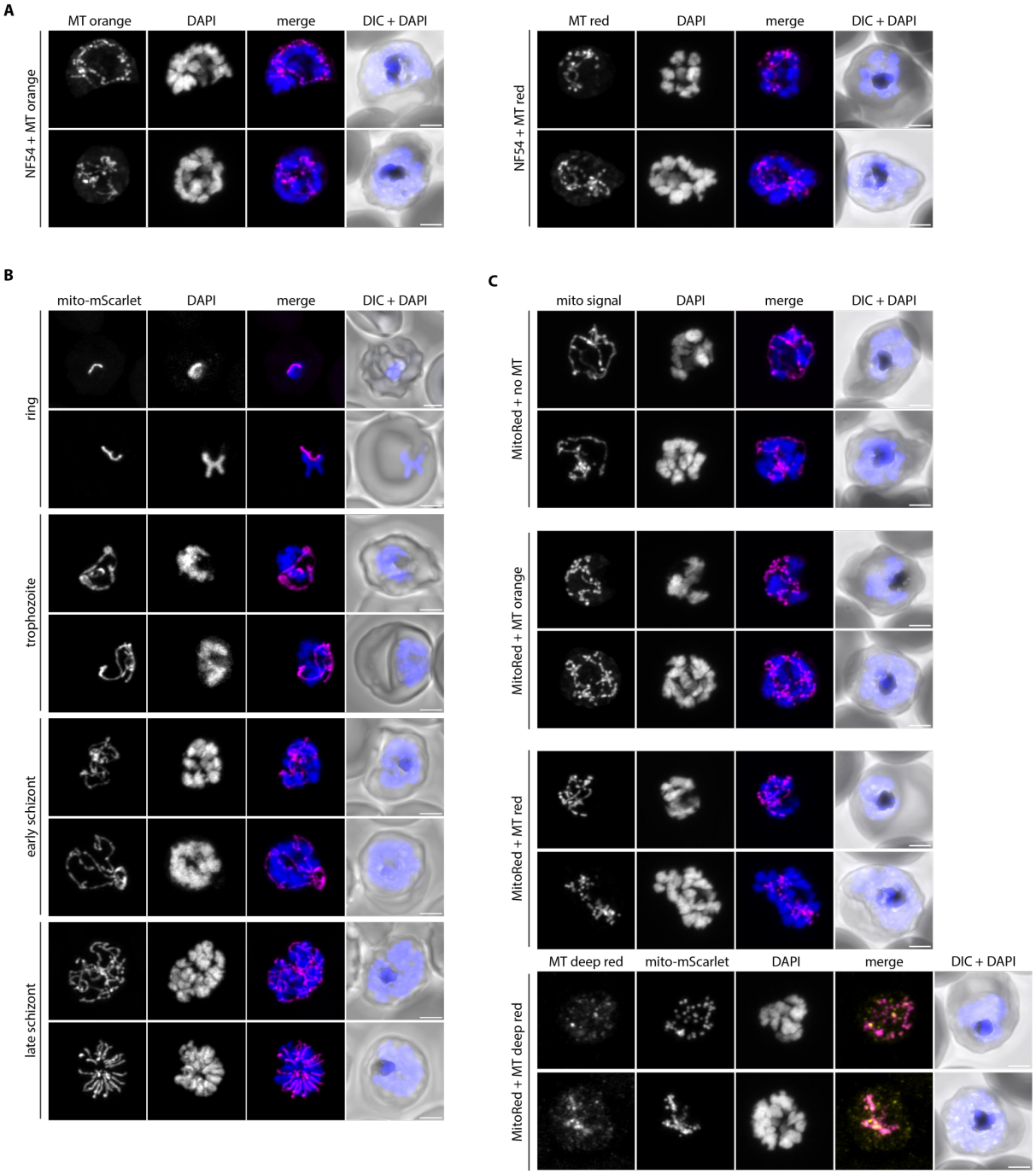

Figure 1. Comparison of MitoTracker and a new mitochondrial marker for fluorescence imaging. *A) Fluorescent imaging of WT parasites stained with MitoTracker Orange CMTMRos (MT orange) or MitoTracker Red CMXRos (MT red). B) Fluorescence microscopy of MitoRed. The mito-mScarlet signal was observed in all asexual life-cycle stages including rings, trophozoites, early and late schizonts. No antibody staining was used and fluorescent signal observed is exclusively the mito-mScarlet signal. C) Fluorescence microscopy of MitoRed, either unstained (no MT) or stained with MT orange, MT red or MitoTracker Deep Red FM (MT deep red). Mito signal is the combined MitoTracker and mito-mScarlet signal that is observed in this channel. All images are maximum intensity projections of Z-stacks taken with Airyscan confocal microscope. Scale bars, 2 μm.*

153 **Mitochondrial dynamics during gametocyte development and activation**
154 To study mitochondrial dynamics throughout the malaria parasite life cycle, MitoRed
155 parasites were induced to form gametocytes, which were fixed for microscopy on day 5, 7,
156 10, and 13 post induction. Parasites were stained for α tubulin to distinguish male and female
157 gametocytes in stage IV and V. In stage II and III gametocytes, the mitochondrion appears as
158 a small knot that increases slightly in size when gametocytes become more mature (Figure
159 2A). This is consistent with our FIB-SEM data[19]. Evers *et al*. also showed that gametocytes
160 have multiple mitochondria already from early gametocyte development onwards. Although
161 light microscopy does not provide the resolution or ability to show membrane boundaries to
162 distinguish the multiple mitochondria in stage II and III gametocytes, in stage IV gametocytes
163 we could clearly observe separate mitochondria in both male and female gametocytes (Figure
164 2A, Figure S3A). There is no clear difference in stage IV gametocytes between male and female
165 mitochondria. However, in stage V gametocytes the mitochondria in males appear slightly
166 more dispersed, while the female mitochondria remain compact (Figure 2A, Figure S3B). Data
167 from Evers *et al.* support this and showed consistently smaller volume and more loosely
168 packed mitochondria in males compared to females[19]. When gametocytes are taken up by
169 the mosquito via a blood meal, they are activated and transform into extracellular male and
170 female gametes. While the female gametocyte develops into a single macrogamete, male
171 gametocytes form up to eight flagellated microgametes. This transformation is triggered by a
172 temperature drop and xanthurenic acid present in the mosquito midgut[20]. Upon *in vitro*
173 activation, the difference between male and female mitochondria becomes more evident.
174 Mitochondria in females remain in a compact knot while the parasite rounds up (Figure 2B).
175 Interestingly, in males the mitochondria become smaller and more dispersed, and sometimes
176 round up to small bean-like structures (Figure 2B, Figure 2D). This process already starts 2
177 minutes after activation. While this particular activation experiment was performed on a
178 gametocyte culture that did not exflagellate for unclear reasons, it was repeated several times
179 and very similar results were found in exflagellating males (Figure 2C). An association of
180 mitochondria with flagella is not uncommon and can also be observed in *e.g.* kinetoplastids,
181 such as *Trypanosoma* and *Leishmania spp*, where the mitochondrion resides at the base of
182 the flagellum, and in human sperm cells, where the mitochondrion wraps around the base of
183 the flagellum to provide energy for flagellar movement[21]. In some exflagellating males, we
184 found close apposition of the dispersed mitochondrion to the axonemes (Figure S4), although
185 this was not consistent.
186
187 **Mitochondrial dynamics in mosquito stages**
188 In the mosquito midgut, the male microgamete seeks out a female gamete for fertilization.
189 After fertilization, the zygote takes one day to transform into a motile ookinete, which can
190 traverse the midgut epithelium and differentiate into an oocyst. This oocyst expands and
191 motile sporozoites are formed within the oocyst. When fully matured, the oocyst will burst
192 and sporozoites will egress, spread through the hemolymph system, and invade the mosquito
193 salivary glands. During oocyst development, the parasite mitochondrion has to expand
194 enormously and then be divided over thousands of daughter sporozoites. However, very little
195 is known about mitochondrial dynamics and only few studies have visualized the
196 mitochondrion during these stages[16,22,23].
197

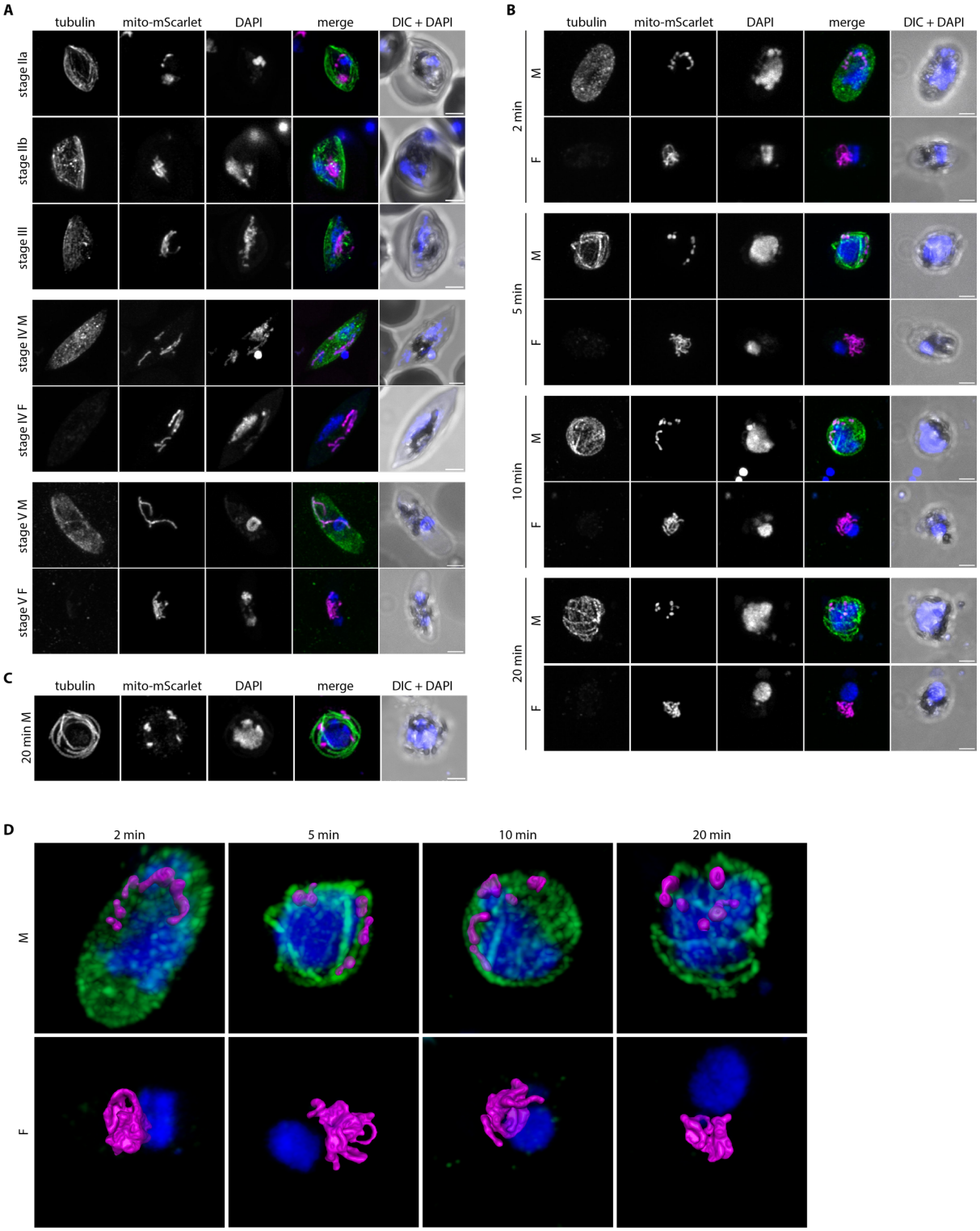

198
199
200 ***Figure 2. Mitochondrial dynamics during gametocyte development and activation.*** *A)*
201 *Immunofluorescence assay on MitoRed gametocytes stages IIa, IIb, III, IV, and V, stained with anti-β-tubulin*
202 *(green) and DAPI (DNA, blue). The mito-mScarlet signal is shown in magenta. In stage IV and V, male (M)*
203 *and female (F) gametocytes are distinguished based on the intensity of the tubulin signal (males high,*
204 *females low). B) Immunofluorescence assay on MitoRed parasites during different stages of gametocyte*
205 *activation (2, 5, 10 and 20 minutes after activation). C) Immunofluorescence assay on MitoRed*
206 *exflagellating male gamete 20 minutes after activation. A-C) Images are maximum intensity projections of*
207 *Z-stacks taken with an Airyscan confocal microscope. Scale bars, 2 μm. D) 3D visualization of male and*

208 *female MitoRed parasites 2, 5, 10, and 20 minutes after activation. The mito-mScarlet fluorescent signal is*
209 *segmented based on manual thresholding.*
210
211 To explore if MitoRed parasites develop normally in the mosquito and to visualize
212 mitochondrial morphology, mature MitoRed gametocytes were fed to *Anopheles stephensi*
213 mosquitoes. One day after the feed, the mosquito blood bolus was extracted and stained with
214 anti-*Pf*s25 conjugated antibodies to visualize ookinetes by live microscopy. We distinguished
215 different stages of ookinete maturation as described by Siciliano *et al.*[24]. Due to the resolution
216 limit of light microscopy, it was difficult to tell if there were one or multiple mitochondria as
217 observed in gametocyte stages. Since we did not find evidence for the presence of multiple
218 mitochondria in these ookinete development stages, we will refer to it as "the
219 mitochondrion" in the coming paragraph, although we cannot rule out the presence of
220 multiple mitochondria. During earlier stages of ookinete development (II), when ookinetes
221 have a short protuberance attached to the round body, the mitochondrion resides in the
222 round body (Figure 3A, 3B). When the protuberance starts to elongate further, one elongated
223 mitochondrial branch stretches out and reaches into the protuberance. In stage III ookinetes,
224 the mitochondrion stretches out further into the growing protuberance, spiraling out from
225 the round body. We could not find clear stage IV ookinetes where the protuberance is at its
226 full length, which could be explained by the swift development from stage IV to V ookinetes
227 as was observed by Siciliano *et al.*[24]. However, in the mature stage V ookinetes, the
228 mitochondrion appears as a tight knot in the main parasite body.
229
230 At day 7, 10, and 13 after infection, mosquitoes from a feed with an infection rate of 100%
231 and an average of 5 oocysts/mosquito were dissected and midguts were used for live confocal
232 microscopy. At day 7, small oocysts were observed with a branched mitochondrial network
233 stretched out throughout the cell (Figure 3C). Segmentation of the fluorescent signal based
234 on manual thresholding indicated that the mitochondrion consisted of one fragment. Day 10
235 oocysts were much larger and the mitochondrial mesh-like network appeared more
236 organized, also localizing to areas directly below the oocyst wall (Figure 3D). At day 13,
237 oocysts of various sizes were observed. Some large oocysts showed a highly organized
238 mitochondrial network, where mitochondrial branches were organized in a radial fashion
239 around a central organizational point (Figure 3E, S5A). We named these points mitochondrial
240 organization centers (MOCs). At least tens of these MOCs could be observed per cell. Some
241 small oocysts at day 13 showed structures that looked like beginning MOCs (Figure S5B).
242 However, several small oocysts showed a dispersed, globular mitochondrial signal, which we
243 interpreted as unhealthy or dying parasite (Figure S5C). While several free sporozoites were
244 observed in dissected midguts and salivary glands on day 16 (data not shown), we never
245 observed an oocyst containing fully mature sporozoites with a divided mitochondrion or an
246 infected salivary gland on day 16 and 21 after infection. This indicates that either the
247 mitochondrial marker itself, or integration in the SIL7 locus causes issues for sporozoite
248 development. We conclude that the MitoRed line is a great tool for mitochondrial
249 visualization in asexual blood stages, gametocytes stages, and mosquito stages up until late
250 oocysts (Supplemental Information S1).
251

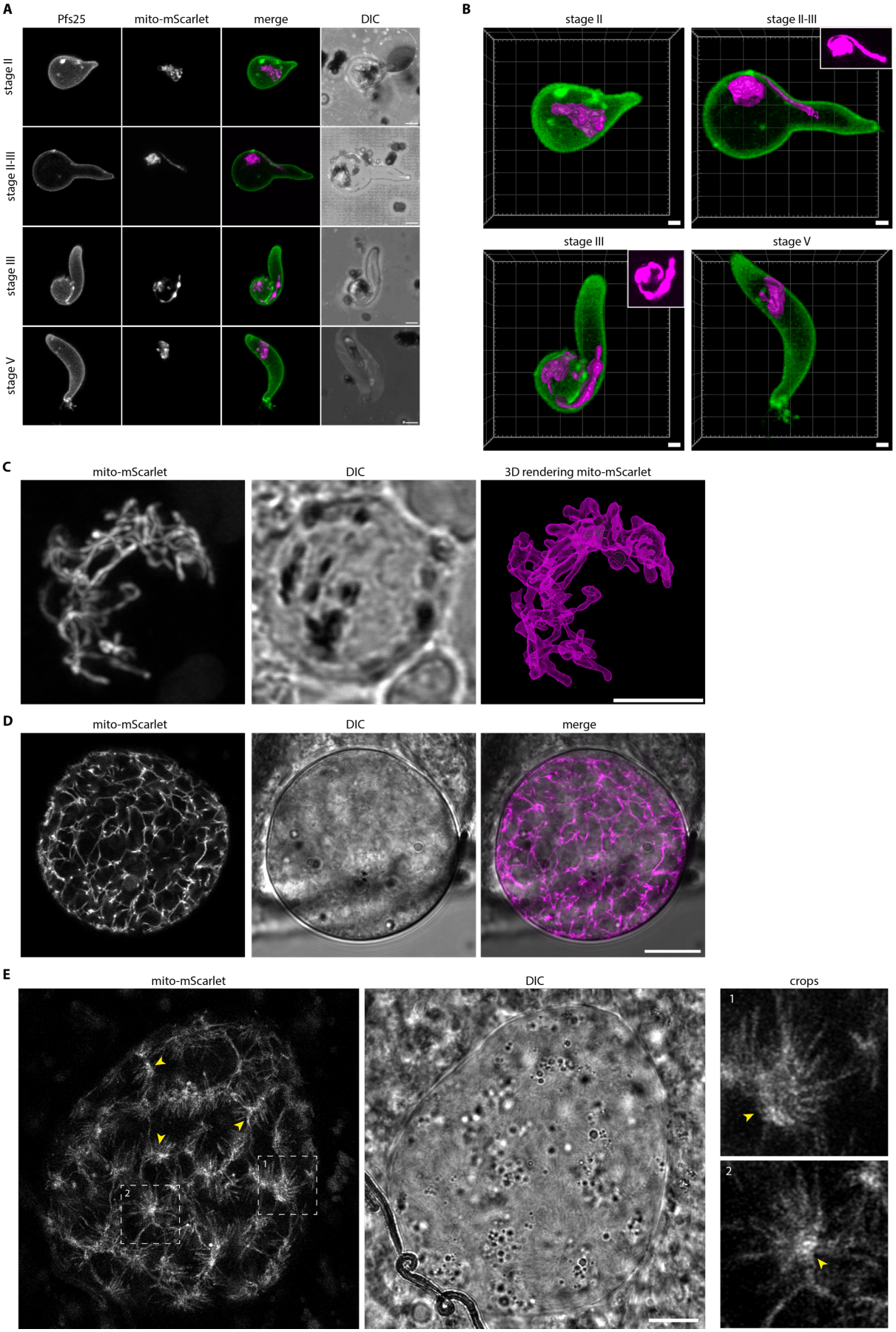
A
Pfs25
mito-mScarlet
merge
DIC
stage II
stage II-III
stage III
stage V
B
stage II
stage II-III
stage III
stage V
C
mito-mScarlet
DIC
3D rendering mito-mScarlet
D
mito-mScarlet
DIC
merge
E
mito-mScarlet
DIC
crops
1
2

252
253

254 ***Figure 3. Mitochondrial dynamics during mosquito stage development.*** *A) Live imaging of MitoRed*
255 *ookinetes one day after mosquito feed. Different stages of ookinete maturation (II – IV) were distinguished*
256 *based on description by Siciliano* et al.[24]*. Cells were stained with an Alexa fluor 488 conjugated anti-Pfs25*
257 *antibody to visualize parasite outline (green). Images are maximum intensity projections of Z-stacks taken*
258 *with an Airyscan confocal microscope. Scale bars, 2 μm. B) 3D visualization of different ookinete maturation*
259 *stages. The mito-mScarlet fluorescent signal is segmented based on manual thresholding. Two smaller*
260 *images in upper right corner of stage II-III and stage III are crops of the mitochondrial fluorescent signal*
261 *with increased brightness and contrast. Scale bars, 1 μm. Live imaging of MitoRed oocysts on day 7 (C) day*
262 *10 (D) and day 13 (E) after mosquito infection. C) Oocyst at day 7 after infection with left image showing a*
263 *maximum intensity projection of the mito-mScarlet signal. Right image shows a segmentation of the mito-*
264 *mScarlet fluorescent signal by thresholding in Arivis software. Scale bar, 4 μm. E) oocyst at day 13 after*
265 *infection. Images on the right are crops of the mito-mScarlet signal of the image on the left, indicated by*
266 *the dotted-line areas. Yellow arrowheads indicate mitochondrial organization centers (MOCs). D-E) Scale*
267 *bars, 10 μm.*
268
269 **Mitochondrial division during schizogony in asexual blood stages**
270 Next, we aimed to use MitoRed for live visualization of mitochondrial division during
271 schizogony in asexual blood stages. The biggest advantage of live imaging is that one parasite
272 can be followed over time to capture mitochondrial fission events chronologically.
273 Unfortunately, this proved to be challenging. All parasites imaged in several experiments for
274 a duration exceeding 60 minutes exhibited significant morphological alterations, including
275 mitochondrial swelling, fragmentation, and formation of vesicle-like structures, which
276 indicate an unhealthy or dying parasite (Figure S6A). Additionally, we frequently observed
277 parasites egressing from their RBCs after approximately 45 minutes of imaging, indicating that
278 imaged parasites are unhealthy (Figure S6B). Optimizing imaging conditions by reducing laser
279 power, increasing time interval, better temperature control, and gassing of the imaging
280 chamber with low oxygen mixed gas (3% O_2, 4% CO_2), did not improve parasite health during
281 imaging. Therefore, we decided to go for a fixed imaging approach to capture mitochondrial
282 division in asexual blood-stages.
283
284 To capture mitochondrial fission, MitoRed parasites were tightly synchronized and fixed
285 between 32-36 and 36-40 hours after invasion. In our culture system, MitoRed parasites have
286 a replication cycle of approximately 40 hours, so we captured the last eight hours of schizont
287 maturation before merozoite egress from the RBC. In order to distinguish the precise stage of
288 schizont maturation, we included an anti-GAP45 antibody staining. Glideosome associated
289 protein 45 (GAP45) is an inner membrane complex (IMC) protein and is important for RBC
290 invasion[25,26]. IMC formation starts at the apical end of a developing merozoite during
291 schizogony and continues to develop until it fully encapsulates the daughter merozoite with
292 its own IMC membrane[27,28]. We used the stage of IMC formation and therefore merozoite
293 segmentation as a marker for the maturity and age of the schizonts. Based on IMC and DNA
294 staining, we differentiated four stages of schizont maturation: pre-segmentation (n=6), early-
295 segmentation (n=9), mid-segmentation (n=15), and late-segmentation (n=10, Figure 4).
296
297 We generated and classified Z-stack images of 40 schizonts, which allowed us to reconstruct
298 a timeline of mitochondrial fission. During pre- and early-segmentation stages, the branched
299 mitochondrial network stretches throughout the parasite. Only at the end of early-
300 segmentation stages, when the IMC is approximately halfway formed, the mitochondrion is
301 oriented around the food vacuole in the center of the parasite with its branches pointing
302 outwards in a radial fashion, creating a "cartwheel"-like structure (Figure 4). As the IMC

303 progresses further and schizonts enter the mid-segmentation stage, this mitochondrial
304 cartwheel structure is divided into smaller fragments, which maintain their radial branch
305 orientation into the segmenting merozoites. Only when IMC formation appears complete, did
306 we observe mitochondria that are entirely divided and distributed over the daughter
307 merozoites. This highlights the extremely late timing of this process.
308

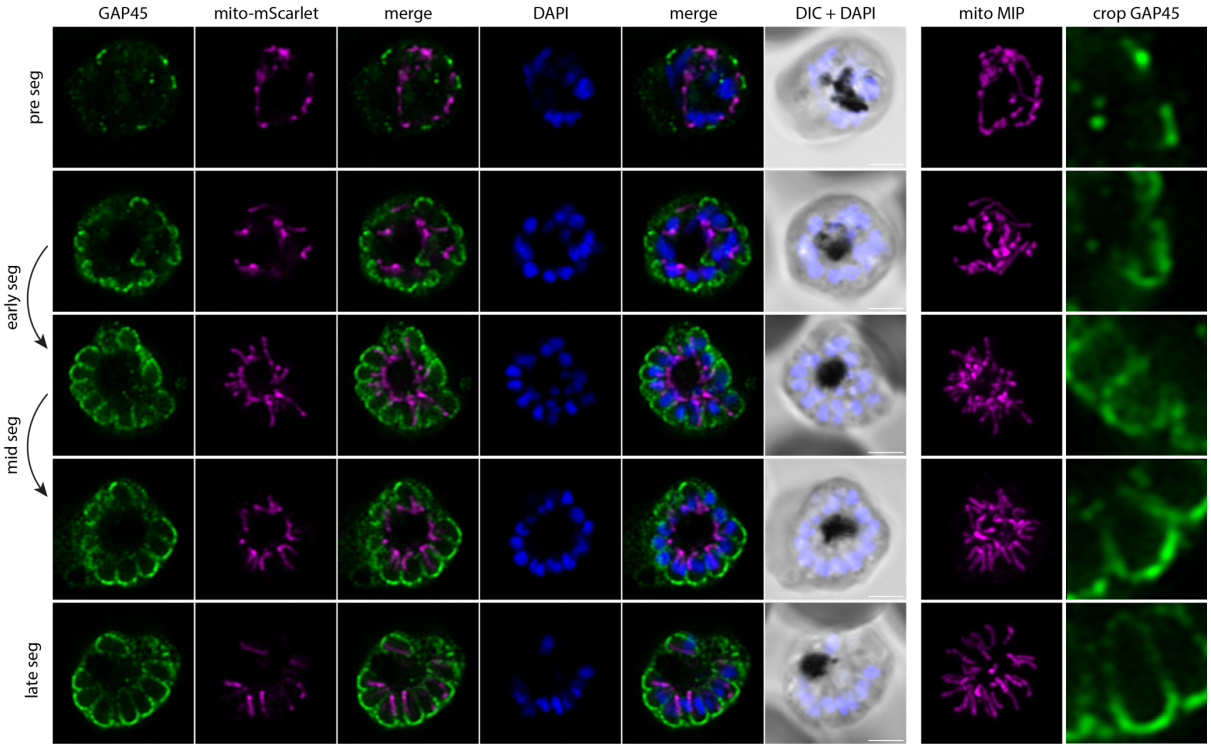

309
310
311 ***Figure 4. Mitochondrial fission in asexual blood-stage parasites.*** *Immunofluorescence assay on MitoRed*
312 *schizonts stained with anti-GAP45 antibody (green) to visualize IMC and DAPI (DNA, blue). The mito-*
313 *mScarlet signal is shown in magenta. Four different stages of schizont maturity are distinguished: pre-*
314 *segmentation (pre seg), schizonts still undergo nuclear division (nuclei are large and irregularly shaped) and*
315 *there is no, or very little IMC staining without clear curvature. Early-segmentation (early seg), schizonts*
316 *have (almost completely) finished nuclear division (nuclei are small and round), there is a clear IMC signal*
317 *that has a curved shape at the apical end of the forming merozoites but is less than half-way formed. Mid-*
318 *segmentation (mid seg), the IMC of the segmenting merozoites in these schizonts is more than half-way*
319 *formed, but there is still a clear opening at the basal end of the merozoite. Late-segmentation (late seg), in*
320 *these schizonts the IMC seems to be completely formed with no clear opening at the basal end of the*
321 *forming merozoites. Images are single slices of a Z-stack taken with an Airyscan confocal microscope.*
322 *Images of the mito-mScarlet signal in the seventh column are maximum intensity projections (MIPs). Images*
323 *in the eighth column are zoom-ins of the GAP45 signal depicted in the first column. Scale bars, 2 μm.*
324
325 To further quantify the numbers and sizes of mitochondria and to create 3D renderings of the
326 mitochondrial network throughout segmentation, we utilized threshold-based masking of the
327 fluorescent signal (Figure 5). During pre- and early-segmentation stages, the mitochondrial
328 network consists of one large fragment (between 7-14 μm^3), often with 1-3 smaller fragments
329 (<1.5 μm^3) (Figure 5AI, 5AII). As evident from our FIB-SEM data (Figure S9A), the
330 mitochondrion features constricted regions, characterized by notably reduced diameters.
331 Hence, the smaller fragments observed during these stages are likely not autonomous but
332 caused by the reduced fluorescent marker intensity in the constricted regions. At the end of
333 early-segmentation stages when the IMC is almost halfway formed, the mitochondrial

network starts to orient itself in a radial fashion around the center of the parasite (Figure 5AII), consistent with the 2D image analysis (Figure 4). During mid-segmentation stages, the radial mitochondrial branches elongate further into the developing merozoites, and the large mitochondrial fragment is divided in smaller fragments at the center of the cartwheel structure (Figure 5AIII). There is a slight increase in number of mitochondrial fragments per parasite, specifically the "intermediate" sized mitochondrial fragments of 1-4 μm^3. Only in the last stage of merozoite segmentation, there is a big increase in the number of mitochondrial fragments (Figure 5C). Of note, there appears to be no correlation between this number and the number of nuclei in the parasites (Figure 5B, 5C). A likely technical explanation is the limited Z-resolution of light microscopy and the different nuclear and mitochondrial segmentation methods. When mitochondrial fragments are located closely above each other, the limited Z-resolution in combination with threshold-based masking can cause the adjacent fragments to appear as one continuous structure. Therefore, the number of mitochondrial fragments per schizonts will be underestimated in these late schizont stages. The nuclei on the other hand were segmented through an automated (spherical) object detection algorithm which does not have this problem. Even when the IMC formation appears to be completed based on the GAP45 staining, only 20% of cells appear to have concluded mitochondrial fission as indicated by exclusively containing homogenously small sized mitochondrial fragments (<1.0 μm^3) (Figure 5AIV). During the late segmentation stage, some parasites still have a large mitochondrial fragment of more than 5 μm^3, while others only have small and intermediate sized mitochondrial fragments (Figure 5D). This suggest that division of the mitochondrial cartwheel structure into small fragments is a fast, stepwise process that does not happen in a 2^n progression and happens only in the final moments of merozoite segmentation.

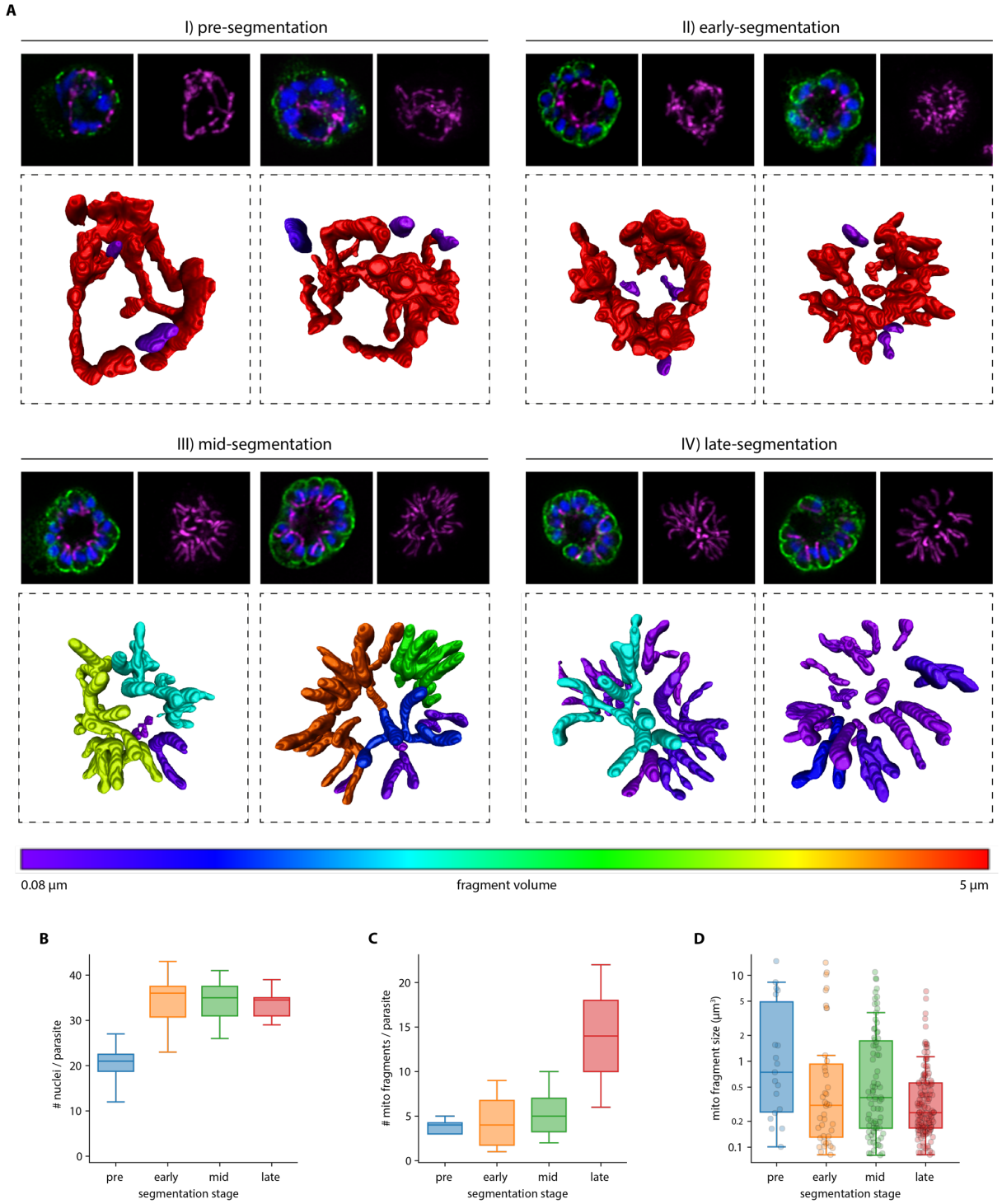

Figure 5. 3D analysis of mitochondrial fission stages during schizogony. *A) 3D visualization of mitochondrial segmentations based on thresholding of the mito-mScarlet signal in Arivis image analysis software. Smaller images in top row are a single slice of the Z-stack with anti-GAP45 labelling (IMC, green), DAPI (DNA, blue) and mito-mScarlet (magenta), and a maximum intensity projection of the mito-mScarlet signal. The larger bottom picture is a 3D visualization of the segmented mitochondrial signal. The color of the mitochondrial fragment represents the size of this fragment, as is shown in the color bar at the bottom. Two representative parasites are depicted for each of the four segmentation stages defined in Figure 4. B) Boxplot indicating the number of nuclei per parasite in the different segmentation stages. C) Boxplot indicating the number of mitochondrial fragments per parasite in the different segmentation stages. D) Boxplot indicating the size of the mitochondrial fragments in the different segmentation stages.*

371 **Visualization of mitochondrial and apicoplast division using volume electron microscopy**
372 Although the use of light microscopy allowed us to reconstruct mitochondrial fission in good
373 temporal resolution, its limited spatial resolution and reliance on indirect staining leaves
374 some questions unanswered. Our recent volume electron microscopy study detailed parasite
375 organelle structures at a nanometer resolution bringing many new insights to the light[19].
376 Here, we reused the underlying FIB-SEM data, which besides gametocytes also contains
377 asexual blood-stage parasites from different stages, to examine mitochondrial fission with
378 high resolution. Asexual parasites in different stages of schizogony were selected and
379 organelles including nuclei, mitochondrion, and apicoplast were segmented for 3D rendering
380 (detailed description per parasite in Tables S2 and S3). In line with the results from our light
381 microscopy experiments, the mitochondrion is a large, branched network stretched
382 throughout the cell in early schizont stages before segmentation has started (Figure 6, Movie
383 1). The apicoplast is also a branched network, however, it is much smaller than the
384 mitochondrion (Table S2). The apicoplast network is divided into smaller fragments of
385 different sizes when nuclear division is still ongoing and IMC formation has started (Figure 7,
386 Table S3, Movie 4). When nuclear division is finishing and the IMC envelops part of the
387 nucleus, apicoplast division is completed (Figure 6, Movie 5). The mitochondrion starts to
388 orient its branches in a radial fashion towards the developing merozoites. When nuclear
389 division is completely finished and the IMC envelops most of the nucleus, the mitochondrion
390 forms a clear cartwheel structure with its branches pointing into the developing merozoites
391 (Movie 6). During late segmentation stages, where only a small opening is connecting the
392 merozoite to the residual body, the mitochondrion is divided into smaller fragments of
393 various sizes (Movie 7). While some mitochondrial fragments have a volume comparable with
394 the mitochondria in a fully segmented parasite (0.016 - 0.036 μm^3), other fragments are still
395 2-4 times that volume (Figure S7).* These larger mitochondrial fragments have several
396 branches that are pointing into developing merozoites but are still connected to each other
397 outside the merozoites. In an almost fully segmented schizont, where most merozoites are
398 fully developed and only few merozoites are still connected to the residual body through a
399 small opening, the mitochondrial division is completed and the number of mitochondrial
400 fragments is the same as the number of merozoites (Movie 8). These findings corroborate our
401 light microscopy data and confirm the mitochondrial division stages, position of relevant
402 structures not stained in light microscopy, and timing of mitochondrial and apicoplast division
403 during schizogony.
404
405 ** Note: The volumes measured in the FIB-SEM data differ greatly from the volumes measured in the 3D*
406 *fluorescent microscopy data. This can be explained by the limited spatial resolution of fluorescent*
407 *microscopy because of the diffraction of light. The diffraction limit of the confocal Airyscan microscope that*
408 *was used is ~120 nm in lateral direction and ~350 nm in axial direction. The diameter of the mitochondrion*
409 *in asexual blood-stage parasites is ~140 nm, which is at the edge of the resolution limit. Therefore, the*
410 *volume measurements of thresholding-based segmentation of the fluorescent signal are not very accurate*
411 *and quickly over-estimate the volume. These volume estimations should merely be used to compare relative*
412 *volumes of mitochondrial fragments. The FIB-SEM data has a resolution of 5 nm in lateral direction and 15*
413 *nm in axial direction, which allows much more precise visualization of organelles and volume*
414 *measurements.*
415

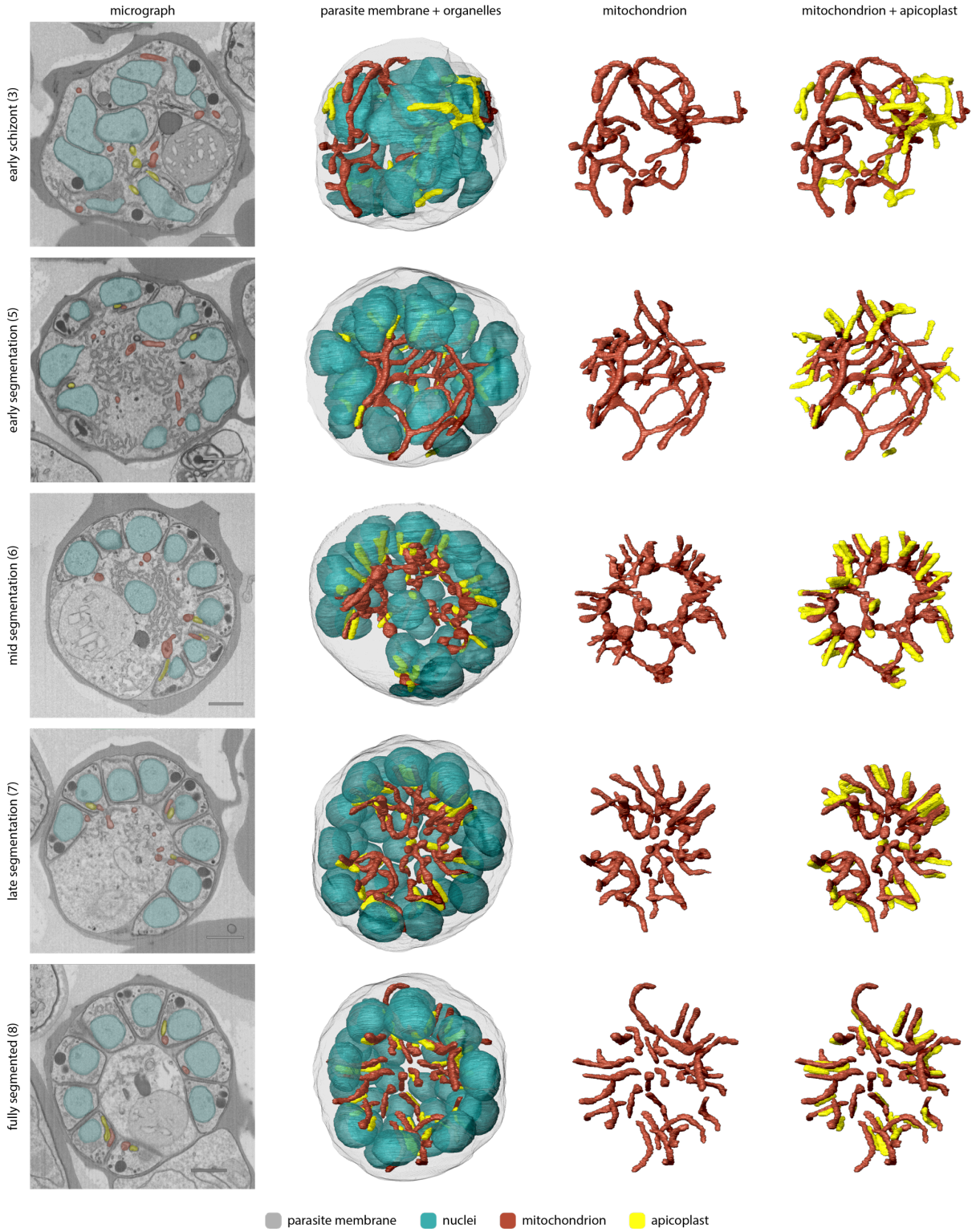

Figure 6. 3D rendering of mitochondrion and apicoplast during different stages of schizogony. *First column contains representative micrograph images from different schizont stages. The numbers between brackets indicate the parasite ID number and detailed information can be found in table S2 and S3. Scale bars, 1 μm. The second, third and fourth column contain 3D renderings of parasite membrane (gray, 5% transparency) nuclei (teal, 50% transparency), mitochondrion (red) and apicoplast (yellow).*

426 **Interaction between mitochondrion and apicoplast in late stage schizonts**
427 During schizogony, the mitochondrion and apicoplast show different moments of close
428 association. Prior to apicoplast division, the mitochondrion and apicoplast have several
429 apposition sites, which have also been described by Evers *et al.*[19] (Figure S8A and S8B). It
430 remains unclear if these close associations represent true membrane contact sites that
431 facilitate the exchange of metabolites or lipids between the organelles, or if these are merely
432 random due to the limited space in the parasite. When apicoplast division is finished, the
433 endings of the mitochondrial branches reach towards the basal endings of the apicoplasts
434 (Figure S8D). Subsequently, the branches of the mitochondrial cartwheel structure align with
435 the apicoplast over its entire length (Figure S8C and S8D). This close alignment remains when
436 mitochondrial division is complete.
437
438 **Bulbous mitochondrial structures with double membrane invaginations**
439 The parasite mitochondrion does not have a consistent diameter during schizogony. While
440 some parts have a very small diameter other areas of the mitochondrion are more bulbous
441 (Figure S9A). These bulbous parts often contain double membrane invaginations of various
442 size and shape (Figure S9C, S9D, S9F). These bulbous invagination structures (bulins) are found
443 in all schizont stages and vary greatly in shape, size, and location in the mitochondrial
444 network. In early stage schizonts, bulins can be found at branching points and in the middle
445 of a continues branch of the mitochondrial network (Figure S9D, S9F). However, during mid-
446 segmentation stages, when the mitochondrion is oriented in its typical cartwheel structure,
447 bulins are consistently observed at the base of a mitochondrial branch near the merozoite
448 entrance (Figure S9D, S9F). These merozoite-entrance bulins were found in all eight mid-
449 segmentation stage schizonts from two independent experiments (example shown in Movie
450 9). Bulbous areas at the base of mitochondrial branches are also observed with fluorescent
451 microscopy (Figure S9B). This, and the specific location of bulins, makes them unlikely an
452 artifact of fixation or sample preparation for the FIB-SEM, although this cannot be ruled out
453 completely. Bulins that reside at the entrance of a forming merozoite during the cartwheel
454 phase are typically characterized by contact with the basal end of the divided apicoplast, and
455 a small constriction right above the bulin where the mitochondrial branch enters the
456 merozoite (Movie 10). Bulbous areas at the base of the mitochondrial branches are also
457 observed with fluorescent microscopy (Figure S9B). In late-segmentation schizonts, we
458 observed small bulins at the base of a divided mitochondrial fragment or at the entrance of a
459 merozoite when the mitochondrial branch was not yet divided (Figure S9D, S9F). Sporadically,
460 we also found bulins in the apicoplast (Figure S9E). The significance and function of these
461 bulins remain to be explored, but it is tempting to speculate about a possible role in organelle
462 division.
463
464 **Centriolar plaques associate with apicoplast but not mitochondrion during organelle**
465 **segregation**
466 In mammalian cells, segregation of organelles is coordinated by microtubules that arise from
467 the centrosomes, or so-called microtubule organizational centers (MTOCs). *Plasmodium*
468 parasites lack canonical centrosomes but organize their mitotic spindle from a structure called
469 the centriolar plaque (CP), which is embedded in the nuclear envelope[29,30]. Expansion
470 microscopy studies from Liffner *et al.* have suggested an association of the CPs with both the
471 mitochondrion and the apicoplast during schizogony, suggesting their involvement in
472 organelle segregation[31]. In our FIB-SEM images, we can distinguish the CP by electron dense

473 coffee filter-shaped regions in the nucleus (Figure 7A). In an early schizont that still lacks IMC
474 or rhoptries, nuclei contain one or two CPs, which are oriented to the periphery of the
475 parasite. 3D renderings show no direct association between the CPs and the mitochondrion
476 or apicoplast (Figure 7B, Movie 1). The distances between the mitochondrion and CPs seems
477 to be significantly smaller than the apicoplast-CPs distances. This can be explained by the fact
478 that the apicoplast is located in the center of the parasite, while the mitochondrion is larger
479 and stretched throughout the whole cell leading to coincidental proximity to the peripheral
480 CPs. In slightly later stage schizonts where IMC and rhoptry formation has started, all nuclei
481 contain either two CPs, or one CP that is dividing. A portion of the CPs associated with the
482 apicoplast, specifically with the endings of apicoplast branches (Movie 2). When the IMC is
483 developed slightly further, all CPs associate with the apicoplast over the total length of the
484 peripherally localized apicoplast network (Movie 3). Usually, two CPs from the same nucleus
485 associate with one apicoplast branch (Figure S10A). However, sometimes two CPs from the
486 same nucleus associate with completely different branches of the apicoplast network (Figure
487 S10B). There does not seem to be a specific association between the mitochondrion and the
488 CPs, and distances between the CPs and apicoplast are significantly smaller compared to the
489 CP-mitochondrion distances (Figure 7B). The association between CPs and apicoplast
490 continues during and after apicoplast division (Movie 4-7). After apicoplast division, each
491 apicoplast fragment is associated with one CP at its peripheral end (Movie 5). During mid-
492 segmentation stages, the endings of the mitochondrial branches are close to the CPs (Movie
493 6). However, this seems to be a result of the close association of the mitochondrion with the
494 apicoplast, rather than a direct interaction between the mitochondrion and the CPs. In a fully
495 segmented schizont, the CPs were much smaller and did not show a clear extranuclear
496 compartment (Movie 8). This close and very consistent association between the apicoplast
497 and the CP, suggest an important role in apicoplast segregation, while the mitochondrion
498 likely deploys different mechanisms to accomplish its proper distribution over the forming
499 merozoites.
500
501
502

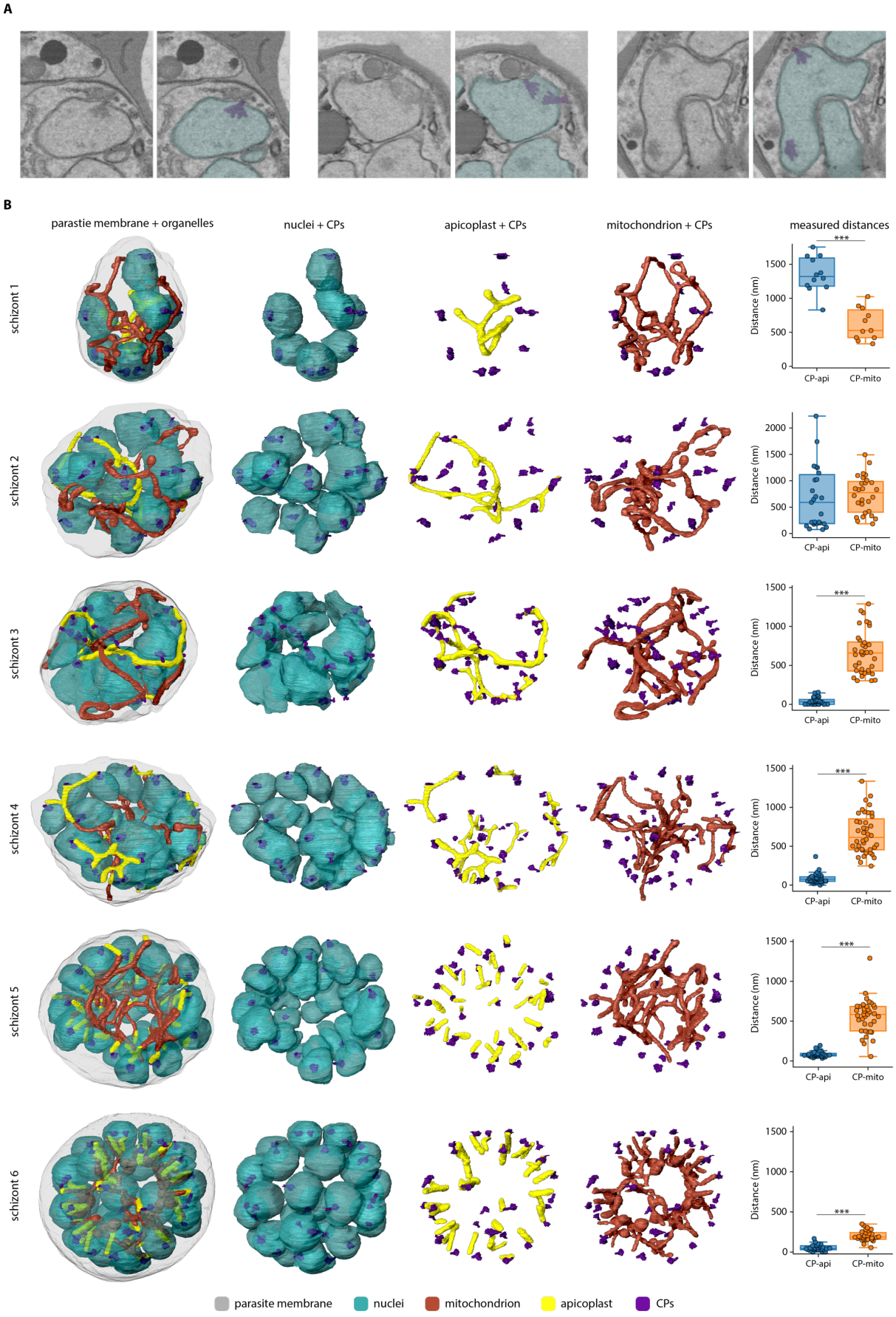
A
B
parastie membrane + organelles
nuclei + CPs
apicoplast + CPs
mitochondrion + CPs
measured distances
schizont 1
schizont 2
schizont 3
schizont 4
schizont 5
schizont 6
Distance (nm)
CP-api
CP-mito
***
parasite membrane
nuclei
mitochondrion
apicoplast
CPs

503
504

Figure 7. Association of apicoplast and not the mitochondrion with centriolar plaques during schizont development. *A) Micrograph images of nuclei (teal) with centriolar plaques (CPs, purple). B) 3D rendering of nuclei (teal), apicoplast (yellow), mitochondrion (red), CPs (purple) and parasite membrane (gray, 5% opacity). Parasite ID numbers are indicated on the left side of the micrograph images. Right column shows measured distances between CPs and closest point to the apicoplast or mitochondrion. *** indicates $p < 0.001$.*

515 ## Discussion

516 In contrast with most eukaryotes, the fast-replicating *P. falciparum* asexual blood-stage
517 parasites harbor only a single mitochondrion. Consequently, proper division and distribution
518 of this organelle during schizogony is crucial to ensure all daughter cells receive a
519 mitochondrion. Here, we visualized the poorly understood mitochondrial dynamics in blood-
520 and mosquito-stages using a new parasite line with a fluorescent mitochondrial marker and
521 super-resolution 3D imaging methods. During blood-stage schizogony, a cartwheel structure
522 is formed and divided into smaller, unequally sized mitochondrial fragments in a stepwise
523 process. Final division into single mitochondria happens during the last stage of merozoite
524 segmentation. These division steps were cross validated by analyzing available FIB-SEM data
525 with nanometer resolution. This also allowed us to reconstruct apicoplast division and its
526 interactions with the mitochondrion. Finally, we showed that the apicoplast but not the
527 mitochondrion associates with the CPs during merozoite formation.
528
529 To date, the visualization of *Plasmodium* mitochondria has largely relied on MitoTracker dyes.
530 However, these dyes are toxic at nanomolar concentrations[14,15] and our data suggest that
531 they may alter mitochondrial morphology (Figure 1). We developed a reporter parasite line
532 harboring a fluorescent mitochondrial marker that shows a more continuous and less
533 punctuated staining pattern compared to MitoTracker dyes and is compatible with live and
534 fixed imaging without necessitating antibody labeling. Unfortunately, MitoRed is not well
535 suited for long-term time lapse imaging (>1h) since parasites showed various signs of poor
536 health, probably due to phototoxicity. While expansion microscopy is currently not feasible
537 with MitoRed, addition of a linear epitope tag would make this marker compatible with the
538 required denaturation step.
539
540 In line with our earlier observations, we demonstrated multiple mitochondria in gametocyte
541 stages[19]. As discussed by Evers *et al.*, there are several possible reasons for the emergence of
542 multiple mitochondria in gametocytes, such as adaptation to a metabolically varied
543 environment, distribution mechanism of mtDNA, or management of reactive oxygen species.
544 We expand upon these observations by also imaging gametocytes during activation. In males,
545 mitochondria become more dispersed while female mitochondria remain in a tight knot. One
546 possible explanation for this is that mitochondria in males are distributed to specific locations
547 in the cell to provide energy locally for certain processes. In sperm cells, the mitochondrion
548 resides at the base of the flagellum to provide energy for flagellar movement[21]. While we
549 observed close apposition of the mitochondria with axonemal tubulin in some activated
550 males using light microscopy (Fig. S4), this was not consistently observed in all males, and we
551 lack the resolution to prove real association. Another explanation could be that the parasite
552 undergoes a form of mitophagy as a source for proteins, lipids, and nucleotides required for
553 the rapid nuclear division and microgamete formation. Even though mitophagy has not been
554 studied in *Plasmodium*, some homologues of the general autophagy pathway have been
555 identified[32]. Autophagy as a survival mechanism was described for *P. falciparum* and *T. gondii*
556 under starvation conditions[33,34]. In *T. gondii*, the fragmentation of the mitochondrion was
557 reversed by using the established autophagy inhibitor 3-methyl adenine[33]. Alternatively, the
558 distribution of the mitochondria could merely be a consequence of the nuclear expansion in
559 the cell.
560

561 Mitochondrial dynamics during mosquito stages is poorly understood and to our knowledge
562 studies have thus far been restricted to *P. berghei*[16,22,23,35]. Here, we visualized the
563 mitochondrion in *P. falciparum* during mosquito stages for the first time. In early oocyst
564 stages, the mitochondrion resembles the extensively branched network from asexual blood-
565 stage schizonts. During oocyst development, the mitochondrial network organizes into
566 multiple MOCs that resemble the cartwheel structure observed in asexual blood stages. In *P.*
567 *berghei* liver-stage schizonts, a very similar mitochondrial organization was observed in sub-
568 compartments created by large membrane invaginations[11,36]. Similar sub-compartments are
569 present during oocyst development[36]. Based on apicoplast visualizations in *P. berghei* and our
570 observations of the formation of MOCs during oocyst stages, mitochondrial and apicoplast
571 dynamics in these sub-compartments in both oocyst and liver stages resemble the dynamics
572 of these organelles in blood-stage schizogony[11,37,38].
573
574 Although the use of new imaging techniques, such as expansion microscopy and 3D volume
575 EM, have revealed new insights in mitochondrial dynamics, many questions about the timing
576 and organization of mitochondrial division remained unanswered[10,31]. In an earlier literature
577 review, we proposed three possible mitochondrial division models: synchronous fission,
578 outside-in fission, or branching point fission[8]. Here, we used a new mitochondrial marker and
579 advanced imaging techniques, such as Airyscan confocal microscopy and FIB-SEM, to
580 reconstruct mitochondrial fission during schizogony, which allows us to propose a new,
581 detailed model for mitochondrial fission (Figure 8). In this model, we describe the cartwheel
582 orientation of the mitochondrion, its non-geometric 2^n division, the late timing of division,
583 and its association with the apicoplast. In other eukaryotic models, mitochondrial fission is
584 facilitated by adaptor proteins on the cytoplasmic side of the outer mitochondrial membrane
585 that recruit dynamin GTPases, which in turn oligomerize to form a constrictive ring around
586 the organelle[8]. *P. falciparum* harbors three dynamins, however, their role in organelle division
587 still needs to be confirmed. The only conserved adaptor protein in *P. falciparum*, Fission 1
588 (Fis1), is dispensable in asexual blood stages precluding an essential role in mitochondrial
589 fission during schizogony[39]. Which proteins comprise the mitochondrial division machinery in
590 *P. falciparum* remains to be explored. The specific location at the entrance of the developing
591 merozoite during mid-segmentation stages could suggest that the bulbous invagination
592 structures, or bulins, could play a role in mitochondrial fission or in the distribution of certain
593 components, e.g. mitochondrial DNA, to the branches of the mitochondrial cartwheel
594 structure that enter the merozoite. However, in earlier stages, bulins are also found at
595 branching points or in continuous parts of the mitochondrion and apicoplast, perhaps
596 suggesting possible roles in more general membrane remodeling of the organellar network.
597
598 The use of volume EM provided the resolution required to verify our fluorescence-based
599 mitochondrial fission model while simultaneously shedding light on the division of the second
600 endosymbiotic organelle, the apicoplast. The apicoplast likely utilizes a similar dynamin-based
601 division machinery as the mitochondrion[8]. As the timing of the apicoplast division precedes
602 that of the mitochondrion, it is even conceivable that (parts of) the same machinery may be
603 reused. The apicoplast divides when nuclear division is still ongoing and merozoite
604 segmentation has just started (Figure 8). Similar to the mitochondrion, its division does not
605 happen in a geometric 2^n progression, but different sized apicoplast fragments are observed
606 in a mid-division stage. The specific types of membrane contact between both endosymbiotic
607 organelles, whether they are direct physical contacts, membrane fusion or tethering, may

608 vary and remain to be explored. The timing and orientation of these organelle appositions,
609 suggest a potential role of the apicoplast in mitochondrial segregation. However, doxycycline
610 treated parasites, that have lost their apicoplast and are chemically rescued by isopentenyl
611 pyrophosphate supplementation, can still produce viable merozoites, suggesting that
612 association with the apicoplast is not essential for mitochondrial segregation[40].
613
614 We also observed CPs, the *P. falciparum* analogue of the centrosome, which function as
615 microtubule organizing centers and are important for mitosis and cell cycle regulation[41,42]. In
616 *T. gondii*, the centrosome associates with the apicoplast and ensures correct segregation of
617 the organelle during daughter cell formation[43,44]. Recent expansion microscopy data
618 suggested interaction of the CP with both the apicoplast and the mitochondrion in *P.*
619 *falciparum*[31]. From the onset of IMC and rhoptry formation, we observed close apposition of
620 the CPs and apicoplast, but not the mitochondrion (Figure 8). This CP-apicoplast association
621 continues during and after apicoplast division, indicating a role of the CPs in apicoplast
622 segregation. The initial absence of CP-apicoplast association and the later association of two
623 CPs from one nucleus with separate apicoplast branches suggests an active recruitment
624 strategy. Motor proteins facilitate intracellular transport of organelles along the cytoskeleton
625 in multicellular eukaryotes. While dynein and kinesin facilitate organelle transport along
626 microtubules, myosin motor proteins transport organelles along actin filaments to specific
627 locations in the cell[45]. Previous studies have shown a critical role of F-actin and myosin F in
628 the inheritance of the apicoplast in *P. falciparum* and *T. gondii*[46–49]. In *T. gondii* parasites that
629 lack myosin F, the apicoplast fails to associate with centrosomes[50]. Therefore, we hypothesize
630 that myosin facilitates recruitment of the apicoplast branches over the actin filaments to the
631 CPs. Although the mitochondrion is close to the CPs in late segmentation stages, the distance
632 is always significantly bigger than the apicoplast-CP distance. Additionally, mitochondrial
633 branches reach much further into the merozoites when fully segmented, compared to the
634 apicoplast. Furthermore, conditional knockout of *Pf*ACT1 (actin-1) did not alter mitochondrial
635 morphology in asexual blood-stage schizogony[46]. Therefore, it remains questionable if the
636 mitochondrial branches are recruited to the CP via a similar mechanism as the apicoplast.
637
638 Volume EM is a powerful tool to study biological questions as it allows the visualization of
639 complex, connecting structures and gives spatial and cellular context. Here, we reused
640 available FIB-SEM data which contains sexual and asexual parasites from many different
641 stages. Future reinterrogation of the data could facilitate in answering other biological
642 questions that are beyond the scope of this paper, such as rhoptry biogenesis and
643 development of the apical complex.
644
645 In this study, we have developed a reporter parasite line harboring a fluorescent
646 mitochondrial marker, integrated in a new genomic locus that can be used for mitochondrial
647 visualization in blood and mosquito stages. This allowed us to visualize mitochondrial division
648 in great detail and describe the relative timing and events of mitochondrial fission and
649 segregation using high-resolution confocal microscopy and FIB-SEM image analysis.
650 Combined with new insights in apicoplast division, mitochondrial and apicoplast interaction,
651 and association of the apicoplast with the CP during schizogony, this allowed us to propose a
652 new, detailed model of apicoplast and mitochondrial division during schizogony. These
653 findings pave the path for more targeted approaches to study the mechanism of
654 mitochondrial and apicoplast division and segregation.

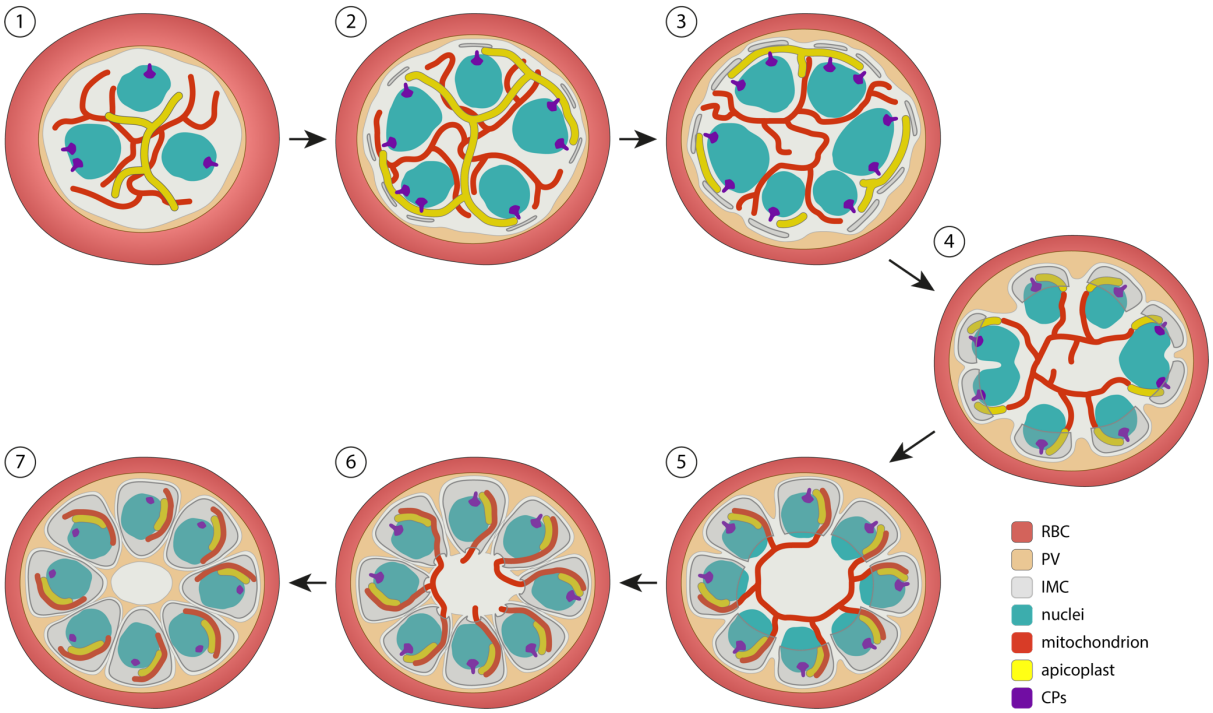

Figure 8. Schematic model for mitochondrial and apicoplast division and segregation in* P. falciparum *during schizogony. *(1) Nuclear division is ongoing, while inner membrane complex (IMC) formation has not started and both the mitochondrion and apicoplast are branched networks. The apicoplast localizes more to the center of the cell, while the mitochondrion is stretched throughout the whole cell. (2) When IMC formation starts, the apicoplast branches associate with the centriolar plaques (CPs) at the periphery of the parasite. (3) The apicoplast divides in a non 2^n progression, while it keeps its interaction with the CPs. (4) When nuclear division is finishing, apicoplast division is completely finished. The apical end of the apicoplast fragments associate with the CPs, while mitochondrial branches associate with the basal end of the apicoplast fragments. (5) The IMC develops further and envelops large parts of the nuclei. The mitochondrion orients itself in a cartwheel structure, while its branches align with the apicoplast fragments. (6) IMC formation is almost finished, and just a small opening connects the merozoites to the residual body. The mitochondrion divides in a non 2^n progression. The apicoplast still associates with the CPs and aligns with mitochondrial branches/fragments. (7) Merozoite segmentation is complete, the apicoplast loses its clear association with the CPs since they become smaller and do not have a clear extra nuclear compartment anymore. The mitochondrion is fully divided and still aligns with the apicoplast. Red blood cell (RBC), parasitophorous vacuole (PV).*

673 # Materials and Methods

674 ***P. falciparum* culture and transfections**

675 *P. falciparum* NF54 and MitoSIL7 parasites were cultured in RPMI1640 medium supplemented
676 with 25 mM HEPES, 10% human type A serum and 25 mM $NaHCO_3$ (complete medium).
677 Parasites were cultured in 5% human RBCs type O (Sanquin, the Netherlands) at 37 °C with 3
678 % O_2 and 4 % CO_2. For transfection, 60 µg of HDR plasmid was linearized by overnight
679 digestion, precipitated, and transfected with 60 µg Cas9 plasmid using ring transfection[51,52].
680 Briefly, a ring-stage sorbitol synchronized parasite culture was transfected with the plasmids
681 by electroporation (310 V, 950 µF). Five hours after transfection, parasites were treated with
682 2.5 nM WR99210 for five days. Success of transfection was assessed by integration PCR (Fig
683 S1, Table S1).
684

685 **Plasmid constructs**

686 To generate the base SIL7 reporter plasmid (pRF0057) the 5' and 3' homology regions for SIL7
687 were amplified from genomic NF54 DNA (Table S1) and cloned into the pBAT backbone with
688 NgoMIV and AleI (5') and BmgBI and AatII (3'). For the final MitoSIL7 repair plasmid, first the
689 mScarlet sequence was amplified from p1.2RhopH3-HA-mScarlet (a kind gift from Prof. Alan
690 Cowman) (Table S1). The mScarlet sequence was cloned into pRF0077 (empty tagging plasmid
691 with PBANKA_142660 bidirectional 3'UTR) with AflII and EcoRI restriction sites, generating
692 pRF0078 intermediate plasmid. The HSP70-3 promotor (prom) and targeting sequence (t.s.)
693 sequence was cloned into pRF0078 with EcoRI and NheI restriction sites, generating pRF0079
694 intermediate plasmid. The whole mitochondrial marker (HSP70-3 prom + t.s. + mScarlet) was
695 cloned from pRF0079 into pRF0057 with EcoRI and AflII restriction sites, generating pRF0191,
696 the final repair plasmid. CRISPR/Cas9 guide plasmids targeting two different sites in the SIL7
697 region were generated. Guide oligonucleotides were annealed and cloned into pMLB626
698 plasmid (a kind gift from Marcus Lee) using BbsI restriction enzyme, generating the two final
699 guide plasmids (Table S1).
700

701 **Growth assay**

702 NF54 WT and MitoSIL7 parasites were synchronized using 63% Percoll centrifugation. Late-
703 stage parasites were isolated from the Percoll gradient and added to fresh RBCs. Four hours
704 later, a 5% sorbitol synchronization was performed, which allowed only young rings that just
705 invaded a new RBC to survive. Ring stage parasites were counted and three independent
706 cultures of 0.05% parasitemia were set up for each parasite line. Every 24 hours, 10 µl culture
707 was taken and fixed in 100 µl 0.25% glutaraldehyde in PBS up until day 5. To prevent
708 overgrowth, parasite cultures were cut back 1/50 after samples were taken on day 3. Before
709 readout, fixative was taken of, and parasite DNA was stained with 1:10,000 SYBR Green in
710 PBS. Parasitemia was determined by measuring SYBR Green positive cells with a Cytoflex flow
711 cytometer (Beckman Coulter Cytoflex) using the 488 nm laser. Final parasitemia of day 4 and
712 5 was adjusted for the 1/50 dilution factor, explaining why final parasitemia can reach more
713 than 100%.
714

715 **Immunofluorescence assays**

716 IFAs were performed on asexual and sexual blood-stage parasites, using the same fixation
717 and staining protocols. Asexual blood-stage parasites were usually synchronized with 5%
718 sorbitol to get them in the preferred stage for the IFAs. For tight synchronization, late-stage
719 parasites were isolated with 63% Percoll centrifugation and added to fresh RBCs. Four hours

720 later, a 5% sorbitol was performed to select for young rings. Parasites were settled on a poly-
721 L-lysine coated coverslip for 20 min at 37 C. Parasites were fixed (4% EM-grade
722 paraformaldehyde, 0,0075% EM-grade glutaraldehyde in PBS) for 20 min and permeabilized
723 with 0.1% Triton X-100 for 10 min. Samples were blocked with 3% bovine serum albumin (BSA)
724 (Sigma-Aldrich) in PBS for 1 h. Primary and secondary antibody incubations were performed
725 for 1 h in 3% BSA. The nucleus was visualized by staining with 1 µM DAPI in PBS for 1 h. PBS
726 washes were performed between different steps. Parasites were mounted with Vectashield
727 (Vector Laboratories). Images were taken with a Zeiss LSM880 or LSM900 Airyscan
728 microscope with 63x oil objective with 405, 488, 561, 633 nm excitations. Images were
729 Airyscan processed before analysis with FIJI software. MitoTracker stainings (including
730 MitoTracker™ Orange CMTMRos, Red CMXRos, Deep Red FM, all from ThermoFisher) were
731 done before settling and fixation by incubation of the parasites with 100 nM MitoTracker for
732 30 minutes at 37 °C, followed by a wash with complete media. The IMC protein GAP45 was
733 labeled using the anti-GAP45 rabbit antibody (1:5000) (a kind gift from Julian Rayner) and
734 goat anti-rabbit AlexaFluor 488 antibody (1:500, Invitrogen). Alfa-tubulin was labeled with an
735 anti-alfa tubulin mouse antibody (1.500, Thermofisher) and chicken anti-mouse AlexaFluor
736 488 antibody (1:400, Invitrogen).
737
738 **Gametocyte generation and mosquito feeds**
739 Gametocyte cultures were maintained in a semi-automatic culturing system with media
740 changes twice a day[53]. MitoRed gametocytes used for imaging were induced by Albumax
741 supplementation. A mixed asexual culture of 1% was set up and cultured in medium
742 supplemented with 2.5% Albumax II (Thermo Fisher Scientific™) without human serum for
743 four days. After four days, parasites were cultured in complete medium again for further
744 gametocyte development. For mosquito feeding, MitoRed gametocytes were stress induced
745 through asexual overgrowing. A mixed asexual culture of 1% was set up and cultured for 2
746 weeks. At day 15 after gametocyte induction, gametocytes were fed to *Anopheles stephensi*
747 mosquitoes (Sind-Kasur Nijmegen strain)[54]. 24 hours after feeding, several mosquitoes were
748 dissected, and blood bolus was obtained for live imaging of ookinetes.
749
750 **Live imaging of asexual blood-stage parasites**
751 Sorbitol-synchronized MitoRed or NF54 schizonts were stained with 0.5 µg/ml Hoechst 33342
752 (Invitrogen, H3570) for 30 minutes at 37 °C for nuclear staining. MitoTracker stainings
753 (including MitoTracker™ Orange CMTMRos, Red CMXRos, Deep Red FM, Rhodamin123, all
754 from ThermoFisher) were done by incubation of the parasites with 100 nM MitoTracker or 1
755 µg/ml Rhodamin123 for 30 minutes at 37 °C, followed by a wash with complete medium.
756 Stained parasites were diluted 1:40 in complete medium and settled for 20 minutes at 37 °C
757 in a poly-L-lysine coated µ-slide 8 well imaging chamber (Ibidi). Unbound cells were washed
758 away with phenol red free complete medium, in which cells were also kept during imaging.
759 Parasites were imaged on a Zeiss LSM880 Airyscan microscope with 37 °C heated stage table
760 and 63x oil objective. Images were Airyscan processed before analysis with FIJI software.
761
762 **Live imaging of mosquito stage parasites**
763 Ookinetes were obtained from the blood bolus of infected mosquitoes 24 hours after feeding.
764 Ookinetes were stained by mouse monoclonal anti-*Pf*s25 conjugated antibody (made in
765 house, final concentration 15µg/ml). Stained sample was applied on a glass slide and covert
766 with a glass coverslip. The sample was immediately imaged on a Zeiss LSM880 Airyscan

767 microscope with 63x oil objective. Mosquito midguts were dissected at day 7, 10, and 13 after
768 infection and put on a glass slide in PBS covert with a glass coverslip. Samples were imaged
769 immediately on Zeiss LSM880 or LSM900 microscope with 63x oil objective. Oocysts were
770 identified based on their fluorescent mitochondrion and round shape in the brightfield
771 channel. All images were Airyscan processed before analysis with FIJI software. 3D
772 segmentations and visualizations were done by manual thresholding of the fluorescent signal
773 in Arivis 4D vision software. Salivary glands were dissected on day 13, 16 and 21 after infection
774 and stained with mouse monoclonal anti-CSP conjugated antibody (made in house, final
775 concentration 1µg/ml). Stained glands were applied on a glass slide and covert with a glass
776 coverslip. Samples were imaged on a Zeiss Axioscope A1 microscope with AxioCam ICc1.
777
778 **FIB-SEM image analysis**
779 FIB-SEM image stacks were reused from Evers *et al.*[19]. For these stacks, gametocyte-induced
780 iGP2 parasite cultures were MACS purified. During this process many late-stage asexual
781 parasites in these cultures were co-purified and fixed in the agarose blocks used for FIB-SEM
782 imaging. Detailed sample preparation and FIB-SEM imaging methods are described in Evers
783 *et al.*[19]. All image processing, visualizations and analysis was done in ORS Dragonfly software
784 (2022.2). Segmentations were done by either manual segmentation or deep learning-based
785 segmentation. Deep learning-based segmentations were manually reviewed and corrected
786 when necessary. 3D renderings of segmented regions were converted to triangle meshes for
787 visualization.

788

789 ## Acknowledgements

790 We thank members from the molecular malaria research group for the discussions. We also
791 thank Aniek Garritsen for her contributions to the generation of the SIL plasmids. We do
792 greatly appreciate the help from Chiara Andolina and Nicholas Proellochs with mosquito
793 experiments. We would like to thank Astrid Pouwelsen, Jolanda Klaassen, Laura Pelser-
794 Posthumus, Saskia Mulder and Jacqueline Kuhnen for breeding of mosquitoes and handling
795 of the infected mosquitoes. We thank the Radboud Technology Center Microscopy, Radboud
796 Technology Center flowcytometry, and Radboudumc Electron Microscopy Center for the use
797 of their facilities. We are grateful to Alan Cowman for sharing the p1.2RhopH3-HA-mScarlet
798 plasmid and Julian Rayner for sharing the anti-GAP45 antibody. J.M.J.V. is supported by an
799 individual Radboudumc Master-PhD grant. A.B.V. is supported by an NIH grant (R01
800 AI028398).

801 # References

802 1. WHO. *World malaria report 2022*. (2022).
803 2. Vaidya, A. B. & Mather, M. W. Mitochondrial evolution and functions in malaria parasites.
804 *Annu. Rev. Microbiol.* **63**, 249–267 (2009).
805 3. Painter, H. J., Morrisey, J. M., Mather, M. W. & Vaidya, A. B. Specific role of mitochondrial
806 electron transport in blood-stage Plasmodium falciparum. *Nature* **446**, 88–91 (2007).
807 4. Ke, H. *et al.* Genetic investigation of tricarboxylic acid metabolism during the Plasmodium
808 falciparum life cycle. *Cell Rep.* **11**, 164–174 (2015).
809 5. Evers, F. *et al.* Composition and stage dynamics of mitochondrial complexes in Plasmodium
810 falciparum. *Nat. Commun.* **12**, 3820 (2021).
811 6. Lamb, I. M., Okoye, I. C., Mather, M. W. & Vaidya, A. B. Unique Properties of Apicomplexan
812 Mitochondria. *Annu. Rev. Microbiol.* **77**, 541–560 (2023).
813 7. Goodman, C. D., Buchanan, H. D. & McFadden, G. I. Is the Mitochondrion a Good Malaria
814 Drug Target? *Trends Parasitol.* **33**, 185–193 (2017).
815 8. Verhoef, J. M. J., Meissner, M. & Kooij, T. W. A. Organelle dynamics in apicomplexan
816 parasites. *MBio* **12**, (2021).
817 9. van Dooren, G. G. *et al.* Development of the endoplasmic reticulum, mitochondrion and
818 apicoplast during the asexual life cycle of Plasmodium falciparum. *Mol. Microbiol.* **57**, 405–
819 419 (2005).
820 10. Rudlaff, R. M., Kraemer, S., Marshman, J. & Dvorin, J. D. Three-dimensional ultrastructure of
821 Plasmodium falciparum throughout cytokinesis. *PLoS Pathog.* **16**, e1008587 (2020).
822 11. Stanway, R. R. *et al.* Organelle segregation into Plasmodium liver stage merozoites. *Cell.*
823 *Microbiol.* **13**, 1768–1782 (2011).
824 12. Linzke, M. *et al.* Live and Let Dye: Visualizing the Cellular Compartments of the Malaria
825 Parasite Plasmodium falciparum. *Cytom. Part A* **97**, 694–705 (2020).
826 13. Painter, H. J., Morrisey, J. M. & Vaidya, A. B. Mitochondrial electron transport inhibition and
827 viability of intraerythrocytic Plasmodium falciparum. *Antimicrob. Agents Chemother.* **54**,
828 5281–5287 (2010).
829 14. Joanny, F., Held, J. & Mordmüller, B. In Vitro activity of fluorescent dyes against asexual blood
830 stages of Plasmodium falciparum. *Antimicrob. Agents Chemother.* **56**, 5982–5985 (2012).
831 15. Gebru, T., Mordmüller, B. & Heldb, J. Effect of fluorescent dyes on in vitro-differentiated,
832 late-stage plasmodium falciparum gametocytes. *Antimicrob. Agents Chemother.* **58**, 7398–
833 7404 (2014).
834 16. Matz, J. M., Goosmann, C., Matuschewski, K. & Kooij, T. W. A. An Unusual Prohibitin
835 Regulates Malaria Parasite Mitochondrial Membrane Potential. *Cell Rep.* **23**, 756–767 (2018).
836 17. Esveld, S. L. Van *et al.* A Prioritized and Validated Resource of Mitochondrial Proteins in
837 Plasmodium Identifies Unique Biology. *mSphere* **6**, e00614-21 (2021).
838 18. Kooij, T. W. A., Rauch, M. M. & Matuschewski, K. Expansion of experimental genetics
839 approaches for Plasmodium berghei with versatile transfection vectors. *Mol. Biochem.*
840 *Parasitol.* **185**, 19–26 (2012).
841 19. Evers, F. *et al.* Comparative 3D ultrastructure of Plasmodium falciparum gametocytes. *bioRxiv*
842 2023.03.10.531920 (2023).
843 20. Billker, O. *et al.* Identification of xanthurenic acid as the putative inducer of malaria
844 development in the mosquito. *Lett. to Nat.* **392**, 289–292 (1998).
845 21. Moraes, C. R. & Meyers, S. The sperm mitochondrion: Organelle of many functions. *Anim.*
846 *Reprod. Sci.* **194**, 71–80 (2018).
847 22. Vega-Rodríguez, J. *et al.* The glutathione biosynthetic pathway of Plasmodium is essential for
848 mosquito transmission. *PLoS Pathog.* **5**, 16–18 (2009).
849 23. Sturm, A., Mollard, V., Cozijnsen, A., Goodman, C. D. & McFadden, G. I. Mitochondrial ATP
850 synthase is dispensable in blood-stage Plasmodium berghei rodent malaria but essential in
851 the mosquito phase. *Proc. Natl. Acad. Sci. U. S. A.* **112**, 10216–10223 (2015).

852 24. Siciliano, G. *et al.* Critical Steps of Plasmodium falciparum Ookinete Maturation. *Front.*
853 *Microbiol.* **11**, 1–9 (2020).
854 25. Ridzuan, M. A. M. *et al.* Subcellular location, phosphorylation and assembly into the motor
855 complex of GAP45 during Plasmodium falciparum schizont development. *PLoS One* **7**, (2012).
856 26. Jones, M. L., Cottingham, C. & Rayner, J. C. Effects of calcium signaling on Plasmodium
857 falciparum erythrocyte invasion and post-translational modification of gliding-associated
858 protein 45 (PfGAP45). *Mol. Biochem. Parasitol.* **168**, 55–62 (2009).
859 27. Rudlaff, R. M., Kraemer, S., Streva, V. A. & Dvorin, J. D. An essential contractile ring protein
860 controls cell division in Plasmodium falciparum. *Nat. Commun.* **10**, 2181 (2019).
861 28. Kono, M., Prusty, D., Parkinson, J. & Gilberger, T. W. The apicomplexan inner membrane
862 complex. *Front. Biosci.* **18**, 982–992 (2013).
863 29. Voß, Y., Klaus, S., Guizetti, J. & Ganter, M. Plasmodium schizogony, a chronology of the
864 parasite's cell cycle in the blood stage. *PLoS Pathog.* **19**, 1–21 (2023).
865 30. Gerald, N., Mahajan, B. & Kumar, S. Mitosis in the human malaria parasite Plasmodium
866 falciparum. *Eukaryot. Cell* **10**, 474–482 (2011).
867 31. Liffner, B. *et al.* Atlas of Plasmodium falciparum intraerythrocytic development using
868 expansion microscopy. *Elife* 1–39 (2023) doi:10.1101/2023.03.22.533773.
869 32. Hain, A. U. P. & Bosch, J. Autophagy in Plasmodium, a multifunctional pathway? *Comput.*
870 *Struct. Biotechnol. J.* **8**, e201308002 (2013).
871 33. Ghosh, D., Walton, J. L., Roepe, P. D. & Sinai, A. P. Autophagy is a cell death mechanism in
872 Toxoplasma gondii Debasish. *Cell. Microbiol.* **23**, 1–7 (2012).
873 34. Joy, S. *et al.* Basal and starvation-induced autophagy mediates parasite survival during
874 intraerythrocytic stages of Plasmodium falciparum. *Cell Death Discov.* **4**, (2018).
875 35. Saeed, S., Tremp, A. Z., Sharma, V., Lasonder, E. & Dessens, J. T. NAD (P) transhydrogenase
876 has vital non-mitochondrial functions in malaria parasite transmission . *EMBO Rep.* **21**, 1–11
877 (2020).
878 36. Burda, P.-C. *et al.* A Plasmodium plasma membrane reporter reveals membrane dynamics by
879 live-cell microscopy. *Sci. Rep.* **7**, 9740 (2017).
880 37. Stanway, R. R., Witt, T., Zobiak, B., Aepfelbacher, M. & Heussler, V. T. GFP-targeting allows
881 visualization of the apicoplast throughout the life cycle of live malaria parasites. *Biol. cell* **101**,
882 415–430 (2009).
883 38. Roques, M., Bindschedler, A., Beyeler, R. & Heussler, V. T. Same, same but different:
884 Exploring Plasmodium cell division during liver stage development. *PLoS Pathog.* **19**, 1–22
885 (2023).
886 39. Maruthi, M., Ling, L., Zhou, J. & Ke, H. Dispensable role of mitochondrial fission protein 1
887 (Fis1) in the erythrocytic development of Plasmodium falciparum. *mSphere* **5**, e00579-20
888 (2020).
889 40. Yeh, E. & DeRisi, J. L. Chemical rescue of malaria parasites lacking an apicoplast defines
890 organelle function in blood-stage Plasmodium falciparum. *PLoS Biol.* **9**, e1001138 (2011).
891 41. Arnot, D. E., Ronander, E. & Bengtsson, D. C. The progression of the intra-erythrocytic cell
892 cycle of Plasmodium falciparum and the role of the centriolar plaques in asynchronous
893 mitotic division during schizogony. *Int. J. Parasitol.* **41**, 71–80 (2011).
894 42. Simon, C. S. *et al.* An extended DNA-free intranuclear compartment organizes centrosome
895 microtubules in malaria parasites. *Life Sci. Alliance* **4**, 1–15 (2021).
896 43. Striepen, B. *et al.* The plastid of Toxoplasma gondii is divided by association with the
897 centrosomes. *J. Cell Biol.* **151**, 1423–1434 (2000).
898 44. van Dooren, G. G. *et al.* A novel dynamin-related protein has been recruited for apicoplast
899 fission in Toxoplasma gondii. *Curr. Biol.* **19**, 267–276 (2009).
900 45. Frederick, R. L. & Shaw, J. M. Moving mitochondria: Establishing distribution of an essential
901 organelle. *Traffic* **8**, 1668–1675 (2007).
902 46. Das, S., Lemgruber, L., Tay, C. L., Baum, J. & Meissner, M. Multiple essential functions of

903 Plasmodium falciparum actin-1 during malaria blood-stage development. *BMC Biol.* **15**, 1–16
904 (2017).
905 47. Periz, J. *et al.* Toxoplasma gondii F-actin forms an extensive filamentous network required for
906 material exchange and parasite maturation. *Elife* **6**, e24119 (2017).
907 48. Stortz, J. F. *et al.* Formin-2 drives polymerisation of actin filaments enabling segregation of
908 apicoplasts and cytokinesis in Plasmodium Falciparum. *Elife* **8**, 1–34 (2019).
909 49. Jacot, D., Daher, W. & Soldati-Favre, D. Toxoplasma gondii myosin F, an essential motor for
910 centrosomes positioning and apicoplast inheritance. *EMBO J.* **32**, 1702–1716 (2013).
911 50. Devarakonda, P. M., Sarmiento, V. & Heaslip, A. T. F-actin and myosin F control apicoplast
912 elongation dynamics which drive apicoplast-centrosome association in Toxoplasma gondii.
913 *MBio* **14**, (2023).
914 51. Wu, Y., Sifri, C. D., Lei, H. H., Su, X. Z. & Wellems, T. E. Transfection of Plasmodium falciparum
915 within human red blood cells. *Proc. Natl. Acad. Sci. U. S. A.* **92**, 973–977 (1995).
916 52. Crabb, B. S. & Cowman, A. F. Characterization of promoters and stable transfection by
917 homologous and nonhomologous recombination in Plasmodium falciparum. *Proc. Natl. Acad.*
918 *Sci. U. S. A.* **93**, 7289–7294 (1996).
919 53. Ponnudurai, T., Lensen, A. H. W., Meis, J. F. G. M. & Meuwissen, J. H. E. Synchronization of
920 Plasmodium falciparum gametocytes using an automated suspension culture system.
921 *Parasitology* **93**, 263–274 (1986).
922 54. Feldmann, A. M. & Ponnudurai, T. Selection of Anopheles stephensi for refractoriness and
923 susceptibility to Plasmodium falciparum. *Med. Vet. Entomol.* **3**, 41–52 (1989).
924